



**INTELLECTUAL  
PROPERTY INDIA**

PATENTS | DESIGNS | TRADE MARKS  
GEOGRAPHICAL INDICATIONS



सत्यमेव जयते

भारत सरकार  
GOVERNMENT OF INDIA

पेटेंट कार्यालय  
THE PATENT OFFICE

पेटेंट प्रमाणपत्र  
PATENT CERTIFICATE  
(Rule 74 Of The Patents Rules)

क्रमांक : 044103567  
SL No :



पेटेंट सं. / Patent No. : 291052  
आवेदन सं. / Application No. : 2563/CHE/2010  
फाइल करने की तारीख / Date of Filing : 03/09/2010  
पेटेंटी / Patentee : INDIAN INSTITUTE OF TECHNOLOGY

प्रमाणित किया जाता है कि पेटेंटी को उपरोक्त आवेदन में यथाप्रकटित REDUCED GRAPHENE OXIDE-BASED-COMPOSITES FOR THE PURIFICATION OF WATER नामक आविष्कार के लिए, पेटेंट अधिनियम, १९७० के उपबंधों के अनुसार आज तारीख 3rd day of September 2010 से बीस वर्ष की अवधि के लिए पेटेंट अनुदत्त किया गया है।

It is hereby certified that a patent has been granted to the patentee for an invention entitled REDUCED GRAPHENE OXIDE-BASED-COMPOSITES FOR THE PURIFICATION OF WATER as disclosed in the above mentioned application for the term of 20 years from the 3rd day of September 2010 in accordance with the provisions of the Patents Act, 1970.



अनुदान की तारीख : 26/12/2017  
Date of Grant :

पेटेंट नियंत्रक  
Controller of Patent

टिप्पणी - इस पेटेंट के नवीकरण के लिए फीस, यदि इसे बनाए रखा जाना है, 3rd day of September 2012 को और उसके पश्चात प्रत्येक वर्ष में उसी दिन देय होगी।  
Note. - The fees for renewal of this patent, if it is to be maintained will fall / has fallen due on 3rd day of September 2012 and on the same day in every year thereafter.



**FORM 2**  
**THE PATENTS ACT, 1970**  
**(39 OF 1970)**  
**&**  
**The Patents Rules, 2003**  
**COMPLETE SPECIFICATION**  
**(Refer section 10 and rule 13)**

**TITLE OF THE INVENTION:**

**REDUCED GRAPHENE OXIDE-BASED-COMPOSITES FOR THE PURIFICATION OF WATER**

**2. APPLICANT:**

**(A) NAME: INDIAN INSTITUTE OF TECHNOLOGY MADRAS**

**(B) NATIONALITY: Indian**

**(C) ADDRESS: INDIAN INSTITUTE OF TECHNOLOGY MADRAS**

**IIT P.O**

**Chennai - 600 036**

**3. Preamble to the Description**

**COMPLETE SPECIFICATION**

The following specification particularly describes the invention and the manner in which is to be performed.

## **FIELD OF INVENTION**

This invention relates to the development of a simple and versatile methodology for making graphene-metal/metal oxide nanocomposites using the inherent reducing ability of reduced graphene oxide. The composites were prepared by simple redox-like reaction between the reduced graphene oxide and the metal precursor(s). The invention also describes a methodology to bind graphene composites on cheap and inert substrates like river sand. The as-synthesized nanocomposites are employed for water purification, more specifically, for the removal of heavy metals from water.

## **PRIOR ART**

Despite the benefits and comforts that chemistry has provided to mankind, we are now facing a great challenge of cleaning the chemical wastes generated during industrial, domestic and agricultural activities, which continue to contaminate our environment. In addition to contaminants generated by human activities, the presence of natural contaminants is also posing great hazard to humanity and its environment, especially in poor countries. It is also unfortunate that water, one of the two essential fluids on which all life depends, is increasingly polluted day by day. Hence, it requires great attention to keep it safe for the benefit of all forms of life on Earth.

Over the years, various technologies have been made to mitigate this problem. Various processes including adsorption, precipitation, membrane separation, amalgamation, and ion-exchange have been tried for this purpose. However, adsorption, an age-old process, but versatile and simple, is proven to be more economical and efficient, especially for removing pollutants from dilute solutions. Numerous adsorbents have been developed for cleaning-up pollutants from water. The efficacy and utility of adsorbents greatly depend upon the affinity of target contaminants towards them and economic viability. Carbon is one such adsorbent, which has been extensively used for this purpose and found to be efficient in scavenging variety of pollutants present in water, be it organic or inorganic. However, to meet the increasingly stringent standard on the quality of drinking water, constant efforts have been carried out to identify better adsorbents. Nanomaterials are new class of materials which offer great possibilities in

adsorbents. Nanomaterials are new class of materials which offer great possibilities in water purification as adsorbents (Savage, N., Diallo, M., Duncan, J., Street, A., Sustich, R., (Ed), *Nanotechnology Applications for Clean Water*. William Andrew, New York, **2008** and the chapters therein, Pradeep, T., Anshup., Noble metal nanoparticles for water purification: A critical review. *Thin Solid Films* **2009**, 517, 6441.). As a result, researchers have focused on nanotechnology for an efficient, cost effective and eco-friendly method to decontaminate water (Dhermendra, K. T., Behari, J., Sen, P., Application of nanoparticles in waste water treatment. *World Appl. Sci J.* **2008**, 3, 417).

Considering that one of the major areas of application of carbon materials historically is water purification, it is important that attempts are made in this direction. Here we investigated a new class of carbon based nanomaterials, namely reduced graphene oxide (RGO) composites for water purification. RGO and its precursor, graphite oxide (GO), as such are interesting materials for various applications including water purification due to their unique two-dimensional nature, band structure, large surface area and various functional groups (Rao, C. N. R., Sood, A. K., Subrahmanyam, K. S., Govindaraj, A., Graphene: the new two-dimensional nanomaterial. *Angew. Chem. Int. Ed.* **2009**, 48, 7752, Geim, A.K., Novoselov, K. S., The rise of graphene. *Nat. Mater.* **2007**, 6, 183, Gil, A. J., Adhikari, S., Scarpa, F., Bonet, J., The formation of wrinkles in single-layer graphene sheets under nanoindentation. *J. Phys. Condens. Matter.* **2010**, 22, 145302, Meyer, J. C., Geim, A. K., Katsnelson, M. I., Novoselov, K. S., Booth, T. J., Roth, S., The structure of suspended graphene sheets. *Nature* **2007**, 446, 60). However, composite materials are known to show superior properties compared to their individual components (Veedu, V. P., Cao, A., Li, X., Ma, K., Soldano, C., Kar, S., Ajayan, P. M., Ghasemi-Nejhad, M. N., Multifunctional composites using reinforced laminae with carbon-nanotube forests. *Nat. Mater.* **2006**, 5, 457, Genqiang, Z., Wei, W., Xiaoguang, L., Enhanced thermoelectric properties of core/shell heterostructure nanowire composites. *Adv. Mater.* **2008**, 20, 3654; Manias, E., Nanocomposites: Stiffer by design. *Nat. Mater.* **2007**, 6, 9.). This is mainly due to synergetic properties that may arise from the combination of the materials. Like many other composites, carbon based composites are reported to show enhanced properties. Various composites of metal

oxide and carbon materials like activated carbon, graphite, carbon nanotubes are being made for different applications (Wu, M., Snook, G. A., Chen, G. Z., Fray, D. J., Redox deposition of manganese oxide on graphite for supercapacitors. *Electrochem. Commun.* **2004**, 6, 499., Ma, S. -B., Ahn, K. -Y., Lee, E. -S., Oh, K. -H., Kim, K. -B., Synthesis and characterization of manganese dioxide spontaneously coated on carbon nanotubes. *Carbon* **2007**, 45, 375). GO and RGO sheets are other interesting carbon based materials for making composites. The first attempt to understand the chemistry of GO was by Boehm et al. where they investigated the catalytic production of HBr (Boehm, H.-P., Clauss, A., Fischer, G. O., Hofmann, U. Z., Adsorption behaviors of extremely thin carbon foils. *Anorg. Allg. Chem.* **1962**, 316, 119). After this, several other attempts have been made to produce GO composites. Compared to GO, RGO composites are fewer in number. Prior art related to GO and RGO composites are given below.

1. Kyotani, T., Suzuki, K., Yamashita, H., Tomita, A., Formation of carbon-metal composites from metal ion exchanged graphite oxide. *Tanso* **1993**, 160, 255.
2. Kovtyukhova, N. I. K., G. A., Chuiko, A. A., Complex formation by transition metal ions in aqueous suspensions of graphite oxide. *Russ. J. Inorg. Chem.* **1992**, 37, 566.
3. Mastalir, A', Kira'ly, Z., Patzko', A', De'ka'ny, I., L'Argentiére, P., Synthesis and catalytic application of Pd nanoparticles in graphite oxide. *Carbon* **2008**, 46, 1631.
4. Mastalir, A', Kira'ly, Z., Benko, M., De'ka'ny, I. Graphite oxide as a novel host material of catalytically active Pd nanoparticles. *Catal. Lett.* **2008**, 124, 34.
5. Stankovich, S., Dikin, D. A., Dommett, G. H. B., Kohlhaas, K. M., Zimney, E. J., Stach, E. A., Piner, R. D., Nguyen, S. T., Ruoff, R. S., Graphene-based composite materials. *Nature* **2006**, 442, 282.
6. Bai, H., Xu, Y., Zhao, L., Li, C., Shi, G., Non-covalent functionalization of graphene sheets by sulfonated polyaniline. *Chem. Commun.* **2009**, 1667.
7. Wang, D.-W., Li, F., Zhao, J., Ren, W., Chen, Z.-G., Tan, J., Wu, Z.-S., Gentle, I., Lu, G. Q., Cheng, H.-M., Fabrication of graphene/polyaniline composite paper via

in situ anodic electropolymerization for high-performance flexible electrode. *ACS Nano* **2009**, 3, 1745.

8. Eda, G., Unalan, H. E., Rupesinghe, N., Amaratunga, G. A. J., Chhowalla, M., Field emission from graphene based composite thin films. *Appl. Phys. Lett* **2008**, 93, 233502.
9. Stankovich, S., Piner, R. D., Chen, X., Wu, N., Nguyen, S. T., Ruoff, R. S., Stable aqueous dispersions of graphitic nanoplatelets via the reduction of exfoliated graphite oxide in the presence of poly(sodium 4-styrenesulfonate). *J. Mater. Chem.* **2006**, 16, 155.
10. Eda, G., Chhowalla, M., Graphene-based Composite thin films for electronics. *Nano Lett.* **2009**, 9, 814-818.
11. Muszynski, R., Seger, B., Kamat, P. V., Decorating graphene sheets with gold nanoparticles. *J. Phys. Chem. C* **2008**, 112, 5263.
12. Si, Y., Samulski, E. T., Exfoliated graphene separated by platinum nanoparticles. *Chem. Mater.* **2008**, 20, 6792.
13. Xu, C., Wang, X., Zhu, J., Graphene-metal particle nanocomposites. *J. Phys. Chem. C* **2008**, 112, 19841.
14. Yoo, E., Okata, T., Akita, T., Kohyama, M., Nakamura, J., Honma, I., Enhanced electrocatalytic activity of Pt subnanoclusters on graphene nanosheet surface. *Nano Lett.* **2009**, 9, 2255-2259.
15. Scheuermann, G. M., Rumi, L., Steurer, P., Bannwarth, W., Mülhaupt, R., Palladium nanoparticles on graphite oxide and its functionalized graphene derivatives as highly active catalysts for the Suzuki-Miyaura coupling reaction. *J. Am. Chem. Soc.* **2009**, 131, 8262.
16. Williams, G., Seger, B., Kamat, P. V., TiO<sub>2</sub>-graphene nanocomposites. UV-assisted photocatalytic reduction of graphene oxide. *ACS Nano* **2008**, 2, 1487.
17. Lambert, T. N., Chavez, C. A., Hernandez-Sanchez, B.; Lu, P.; Bell, N. S.; Ambrosini, A., Friedman, T., Boyle, T. J., Wheeler, D. R., Huber, D. L., Synthesis and characterization of titania-graphene nanocomposites. *J. Phys. Chem C* **2009**, 113, 19812

18. Williams, G., Kamat, P. V., Graphene-semiconductor nanocomposites: excited-state interactions between ZnO nanoparticles and graphene oxide. *Langmuir* **2009**, *25*, 13869.
19. Wang, D., Choi, D., Li, J., Yang, Z., Nie, Z., Kou, R., Hu, D., Wang, C., Saraf, L. V., Zhang, J., Aksay, I. A., Liu, J., Self-assembled TiO<sub>2</sub>-graphene hybrid nanostructures for enhanced Li-ion insertion. *ACS Nano* **2009**, *3*, 907.
20. Wang, X., Tabakman, S. M., Dai, H., Atomic layer deposition of metal oxides on pristine and functionalized graphene. *J. Am. Chem. Soc.* **2008**, *130*, 8152.
21. Zheng, W. T., Ho, Y. M., Tian, H. W., Wen, M., Qi, J. L., Li, Y. A., Field emission from a composite of graphene sheets and ZnO nanowires. *J. Phys. Chem C* **2009**, *113*, 9164.
22. Tung, V. C., Chen, L.-M., Allen, M. J., Wassei, J. K., Nelson, K., Kaner, R. B., Yang, Y., Low-temperature solution processing of graphene-carbon nanotube hybrid materials for high-performance transparent conductors. *Nano Lett.* **2009**, *9*, 1949.
23. WO 2009/143405 A3-Synthesis of graphene sheets and nanoparticle composite of the same.
24. United States patent 2010/0036023 A1- Graphite nanocomposites.
25. United States patent 2006/0191835 A1- Compositions and methods of remediations devices with nanostructures sorbents
26. United States patent 2010/0081587 A1-Nanocomposites of graphene and metal oxide materials.
27. United states patent 2010/0096597 A1-Funcional graphene-rubber nanocomposites
28. United States patent 2009/0036605 A1-Oilefield nanocomposite.
29. United States patent 2010/0096595 A1-Functional graphene-polymer nanocomposite for gas barrier applications.
30. United States patent 2010/0021819 A1-Graphene composties for electrochemical cell electrodes.
31. United States patent 2006/0122451 A1-Binding and in situ destruction of chemical agents and other contaminants

### 32. United States patent 2009/0020764 A1-Graphene-based transistor.

All these composites were proposed for either catalytic or electronic applications. Very recent literature reports the synthesis of GO-MnO<sub>2</sub> and graphene-MnO<sub>2</sub> composites and its utility as super capacitor (Sheng, C., Junwu, Z., Xiaodong, W., Qiaofeng, H., Xin, W., Graphene oxide-MnO<sub>2</sub> nanocomposites for supercapacitors. *ACS Nano* **2010**, *4*, 2822.; Jun, Y., Zhuangjun, F., Tong, W., Weizhong, Q., Milin, Z., Fei, W., Fast and reversible surface redox reaction of graphene-MnO<sub>2</sub> composites as supercapacitor electrodes. *Carbon* **2010**, doi:10.1016/j.carbon.2010.06.047). Recent efforts also show that graphene composites like graphene-Fe<sub>3</sub>O<sub>4</sub> and GO-Fe(OH)<sub>3</sub> are efficient in arsenic removal (Chandra, V., Park, J., Chun, Y., Lee, J. W., Hwang, I.-C., Kim, K. S., Water-dispersible magnetite-reduced graphene oxide composites for arsenic removal *ACS Nano* **2010**, *4*, 3979.; Zhang, K., Dwivedi, V., Chi, C., and Zhang, J. W., Graphene oxide/ferric hydroxide composites for efficient arsenate removal from drinking water *J. Hazard. Mater.* **2010**, doi:10.1016/j.jhazmat.2010.06.010). Water, being universal solvent, is affected by a number of contaminants and those contaminants are regulated as per drinking water norms [<http://www.epa.gov/safewater/contaminants/index.html>]. Therefore, more efforts have to be made to find suitable combination of materials and methods to effectively address diverse contaminants.

The methodologies adopted in most of the previous methods for composites formation are relatively cumbersome. The precursor was separately prepared and mixed or external aids were employed for the production of composites. Recently, Kong et al. reported a convenient method for the preparation of RGO-Au composite by using vacuum filtration (Kong, B.-S., Geng, J., Jung, H.-T., Layer-by-layer assembly of graphene and gold nanoparticles by vacuum filtration and spontaneous reduction of gold ions *Chem. Commun.* **2009**, 2174). Later Zhou et al. reported a RGO-Ag composite produced through a one-step chemical method at 75 °C (Zhou, X., Huang, X., Qi, X., Wu, S., Xue, C., Boey, F. Y. C., Yan, Q., Chen, P., Zhang, H., In situ synthesis of metal nanoparticles on single-layer graphene oxide and reduced graphene oxide surfaces *J. Phys. Chem. C* **2009**, *113*, 10842). They adsorbed GO or RGO on 3-aminopropyltriethoxysilane (APTES)-modified Si/SiO<sub>x</sub> substrate and heated the sample



in an aqueous solution of silver nitrate at 75 °C. A novel approach has been reported here to synthesize monodispersed and uncapped nanoparticles of environmental interest such as silver, gold, platinum, palladium and manganese oxide on the surfaces of RGO. An *in-situ* homogenous reduction strategy utilizing the inherent reducing ability of RGO to produce composite materials was explored, at room temperature, without any external aids, in a homogenous solution. The simple methodology adopted here permits to make large-scale RGO nanocomposites with good control over the particle size, which is very important for mass application like water purification.

### ***Supported nanomaterials for water purification***

Apart from efficacy, other important aspect of practical adaptability of any materials for the large-scale and down to earth application like water purification is the cost and the ease of operation. Though, nanomaterials offers great efficacy over their counter parts, one of the critical problems of field adaptability of nanomaterials for water purification is the handling of the adsorbent material after post treatment. Easy solid-liquid separation without any external aid is a must. The best approach for this is to support them on suitable matrices, preferably cheap, stable in water under various conditions, and non toxic, for adaptability in the field for application like water purification. Various supported nanomaterials are reported in literature for water purification. They often show improved performance and multitasking ability. Recent research by our group showed that nanomanganese oxide supported on cellulose fibers are superior candidate for lead removal from water (Maliyekkal, S. M., Lisha, K. P., Pradeep, T., A novel cellulose-manganese oxide hybrid material by *in-situ* soft chemical synthesis and its application for the removal of Pb(II) from water *J. Hazard. Mat.* **2010**, *181*, 986). In our earlier work, we also demonstrated that noble metal nanoparticles can effectively immobilize on supports like alumina and can be used as an efficient and cost effective medium for removal of contaminants like pesticide and mercury (T. Pradeep and S. Nair, Extraction of malathion and chlorpyrifos from drinking water by nanoparticles-Adsorbent composition, a device and a method for decontaminating water containing pesticides, PCT application, PCT/IN05/0002; T. Pradeep and S. Nair, A method of preparing purified water from water containing pesticides (chlorpyrifos and malathion) and purified

water prepared by the said method, Indian patent 200767, Pradeep, T., Nair, S.K., Polyurethane foam coated with silver nanoparticles; Indian patent, 20070608, Pradeep T., Nair, S.K., A method to produce supported noble metal nanoparticles in commercial quantities for drinking water purification, 1879/CHE/2007; Lisha, K. P., Anshup, Pradeep, T., Towards a practical solution for removing inorganic mercury from drinking water using gold nanoparticles, *Gold Bulletin* **2009**, 42,144). More details on the impregnation of metal nanoparticles on various supports are described elsewhere (Noble metal nanoparticles for water purification: A critical review Pradeep, T., Anshup, *Invited critical review. Thin Solid Films* **2009**, 517, 6441). The reports clearly show that nanoparticles can be effectively employed in the field by appropriate immobilization techniques.

Considering all these aspects, we have developed a new material essentially consists of RGO-metal/metal oxide nanocomposites. The composites were prepared by a simple redox-like reaction between RGO and metal precursor using inherent reducing ability of RGO). A simple methodology was developed to effectively support GO/RGO/RGO-composites on RS. Chitosan, an abundantly available and environment-friendly biomaterial was used as a binder for this process. This helps in easy separation of the adsorbent from the aqueous medium, otherwise laborious processes like high speed centrifugation or membrane filtration, or magnetic separation are required, which are not practical for many end-users.

#### **DESCRIPTION OF THE INVENTION:**

In the following, we present a versatile in-situ method for the production of a hybrid material essentially consisting of RGO and a metal/metal oxide. The process of synthesis was conducted in water medium at room temperature. The uptake capacities of the as-made composites were tested for heavy metals from water and are presented. However, the result presented here should not be construed as limiting the scope of the invention.

## **Experimental Methods**

### ***Material characterization***

Surface morphology, elemental analysis and elemental mapping studies were carried out using a Transmission Electron Microscope (TEM) equipped with Energy Dispersive Analysis of X-rays (EDX) (INCA, Oxford Instruments, UK). For this, the sample prepared as mentioned above was drop casted on an amorphous carbon films supported on copper grids and dried at room temperature. Samples were characterized using Scanning Electron Microscope (SEM) (FEI quanta 200) as well. The samples prepared as above were spotted on indium tin oxide (ITO) conducting glass and dried. High resolution Transmission Electron Microscopy (HRTEM) images of the sample were obtained with JEM 3010 (JEOL JEM 3010, Japan). X-ray Photoelectron Spectroscopic (XPS) analysis was done using ESCA Probe TPD of Omicron Nanotechnology. Polychromatic Mg K $\alpha$  was used as the X-ray source ( $h\nu = 1253.6$  eV). Spectra in the required binding energy range were collected and an average was taken. Beam induced damage of the sample was reduced by adjusting the X-ray flux. Binding energy was calibrated with respect to C 1s at 284.5 eV. UV/Vis spectra were measure using Lambda 25 spectrometer (Perkin-Elmer, USA). Samples were characterized using Raman spectroscopy also (WiTec GmbH CRM 200, Germany)

### **Example 1**

GO synthesis from graphite powder was carried out based on the modified Hummers method reported by Kovtyukhova et al. (Hummers, W. S., Offeman, R. E., Preparation of graphitic oxide. *J. Am. Chem. Soc.* **1958**, *80*, 1339.; Kovtyukhova, N. I., Ollivier, P. J., Martin, B. R., Mallouk, T. E., Chizhik, S. A., Buzaneva, E. V., Gorchinskiy, A. D., Layer-by-layer assembly of ultrathin composite films from micron-sized graphite oxide sheets and polycations. *Chem. Mater.* **1999**, *11*, 771). The volumes were scaled up to match our requirements. Complete oxidation was ensured by preceding the actual oxidation by a pre-oxidation step. The pre-oxidized graphite is reported to undergo complete oxidation during the oxidation step to form GO. Detailed procedure is reported

elsewhere. (Kovtyukhova, N. I., Ollivier, P. J., Martin, B. R., Mallouk, T. E., Chizhik, S. A., Buzaneva, E. V., Gorchinskiy, A. D., Layer-by-layer assembly of ultrathin composite films from micron-sized graphite oxide sheets and polycations. *Chem. Mater.* **1999**, *11*, 771).

The GO reduction was carried out similar to a procedure reported by Li et al. (Li, D.; Muller, M. B., Gilje, S., Kaner, R. B., Wallace, G. G., Processable aqueous dispersions of graphene nanosheets. *Nat. Nanotech.* **2008**, *3*, 101). Briefly, GO was exfoliated by sonication and hydrazine hydrate solution (35 wt% in water) was added and stirred. The solution was made alkaline by the addition of ammonia solution (28 wt% in water). The mixture was heated at 90 °C. The reduction of GO to RGO happens in about 2h. Detailed procedure for the reduction and the post reduction processing is reported elsewhere (Li, D., Muller, M. B., Gilje, S., Kaner, R. B., Wallace, G. G., Processable aqueous dispersions of graphene nanosheets. *Nat. Nanotech.* **2008**, *3*, 101). This sample will be referred as purified reduced graphene oxide sheets (RGO).

25 mL of RGO were taken in a 50 mL beaker and calculated volumes of the metal ion precursors ( $\text{KMnO}_4$ ,  $\text{HAuCl}_4$ ,  $\text{AgNO}_3$ ,  $\text{H}_2\text{PtCl}_6$ ,  $\text{PdCl}_2$ ) were added such that the final concentration in the solution was 0.01, 0.025, 0.05, 0.1, 0.3 mM, etc. This was incubated undisturbed for 12 h at 30 °C. Later, all the solutions were put for dialysis against distilled water for 5 days. After dialysis, the samples were stored in glass bottles for further use. This produces RGO composites.

## Example 2

In order to support RGO composites on RS, the following protocol was adopted. Initially, as-prepared RGO- $\text{MnO}_2$ /RGO-Ag and chitosan (Ch) solution (0.8 % chitosan in 1.5 % acetic acid) were mixed in 1:1 ratio. The mixture was stirred thoroughly to obtain a homogenous dispersion. 25 mL of the homogeneous dispersion was added to 10 g of RS and mixed thoroughly. The mixture was dried at 40 °C under constant stirring to ensure uniform coating. To stabilize the coating, the dried samples were soaked in ammonia solution (35 %) for 1 h and subsequently washed with distilled water until the

pH of the wash water become nearly neutral. The materials were dried at 40 °C overnight and stored in glass bottles for further use.

### **Example 3**

Two model RGO composite systems (i.e. RGO-MnO<sub>2</sub> and RGO-Ag), both in supported and unsupported form were evaluated for their utility in Hg(II) removal from aqueous medium. The Hg(II) uptake capacities of various other adsorbents, including RGO, activated carbon (AC), Ag impregnated carbon (AC-Ag), MnO<sub>2</sub> impregnated carbon (AC-MnO<sub>2</sub>), RS, Chitosan (Ch) were compared with RGO-composites. For this, batch adsorption experiments were carried out in 20 mL glass bottles and the working volume was maintained as 10 mL. Homogenous adsorbent dispersion were taken in the reactor and the target pollutant was spiked into this solution to get the required concentration (1 mg/L) of Hg(II). For supported RGO composites immobilized on RS, 250 mg of adsorbent was weighed and added to 10 mL of 1 mg/L of Hg(II) solution. In all the cases, solutions were kept for stirring at 30 ± 2 °C. The samples were collected at predetermined time intervals and analyzed for residual mercury concentrations. The solid-liquid separation was done either by membrane filtration or by simple settling depending upon the adsorbents employed. The filtration protocol consists of filtering adsorbent dispersion through a 200 nm membrane filter paper (Sartorius stedim biotech, Sartorius biolab Products) followed by 100 nm anodized filter paper (Whatman, Schleicher and Schuell). For conducting adsorption experiments in real water, the water was simulated by spiking ~1 mg/L of Hg(II) into a groundwater. The water quality characteristics of ground water are given in Table 1. In order to test the specificity of Hg(II) removal from the aqueous medium in presence of other heavy metals (Ni(II), Cd(II) and Cu(II)), selective metal ion adsorption tests were performed by using a mixture of aqueous solution of ~1.0, 2.0 and 5.0 mg/L of each four metal ions by following the procedure given above. The residual metal ion concentrations present in solution were determined by using a PerkinElmer 5300 DV series Inductively Coupled Plasma (ICP-AES) analyzer.



## DRAWINGS AND TABULATED DATA

Figure 1. UV/Vis spectra of RGO upon the addition of metal ions. A)  $\text{KMnO}_4$ , B)  $\text{Au}^{3+}$ , C)  $\text{Ag}^+$ , and D)  $\text{Pt}^{2+}$ . Absorption at 270 nm for RGO and the changes due to the formation of  $\text{MnO}_2$ , Au, Ag and Pt nanoparticles can be seen. Spectral changes are marked. Pt nanoparticles do not show a distinct plasmon absorption.

Figure 2. A) and B) Large area TEM image of RGO showing the characteristic wrinkles and edges of  $\sim 1$  nm confirming the graphenic nature of the sample. C) and D) TEM images of RGO- $\text{MnO}_2$  (0.05 mM) showing at various magnifications nanoparticles attached to RGO. Folded RGO sheets are marked with arrows in C.

Figure 3. TEM images of RGO-Ag (0.05 mM) showing well dispersed nanoparticles over a RGO sheet.

Figure 4. TEM images A) 0.01 mM B) 0.02 mM C) 0.07 mM RGO-Au sample. Inset of B shows a high magnification lattice resolved image of the 0.02 mM sample with slightly non-spherical structure. D) SEM image of an aggregated sample (0.1 mM), of RGO-Au.

Figure 5. A) TEM image of the RGO-Pt sample containing 0.02 mM  $\text{H}_2\text{PtCl}_4$ . B) Lattice resolved image of the same sample showing the lattice structure of Pt nanoparticles. C) and D) SEM images taken from the aggregated sample of higher concentration (0.1 mM).

Figure 6. SEM images of RGO-Pd samples: A) 0.025 mM and B) 0.1 mM of  $\text{PdCl}_2$ . C) EDS spectrum taken from the sample containing 0.1 mM  $\text{PdCl}_2$ .

Figure 7. Concentration dependent TEM images of RGO- $\text{MnO}_2$ . A1) 0.01 mM, A2) 0.025 mM and A3) 0.05 mM and RGO-Ag B1) 0.01 mM, B2) 0.025 mM and B3) 0.05 mM. Insets in all figures show the lattice resolved images taken from the same sample. All scale bars in the inset correspond to 5 nm.

Figure 8. Raman spectrum of RGO-MnO<sub>2</sub> sample showing the presence of MnO<sub>2</sub> in the composite.

Figure 9. Raman spectra of A) RGO-MnO<sub>2</sub> composite and B) RGO-Ag composite, at different loading of MnO<sub>2</sub> and Ag. Peak positions are marked.

Figure 10. XPS spectra of samples containing 1) 0.025 mM, 2) 0.05 mM and 3) 0.1 mM KMnO<sub>4</sub>. A) C 1s, B) O 1s, and C) Mn 2p regions.

Figure 11. XPS spectra of RGO-Ag composite. A) C 1s and B) Ag 3d. In the C 1s spectra, we can see that as the concentration of AgNO<sub>3</sub> increased, the extent of oxidation of carbon is also increased. Ag 3d<sub>5/2</sub> is at the metallic value of 368 eV.

Figure 12. SEM Images of A) Ch-RGO-Ag@RS, B) Ch-RGO-MnO<sub>2</sub>@RS; inset in A shows an SEM image of bare sand particles before coating. C) Raman spectrum of (a) RS, (b) Ch, C) Ch-RGO-MnO<sub>2</sub>@RS and (d) Ch-RGO-Ag@RS. D) Photograph of RS, Ch-RGO-MnO<sub>2</sub>@RS and Ch-RGO-Ag@RS showing the color change.

Figure 13. EDAX analysis of Ch-RGO-Ag@RS composite.

Figure 14. EDAX analysis of Ch-RGO-MnO<sub>2</sub>@RS composite.

Figure 15. A) Comparison of  $K_d$  values obtained for the adsorption of Hg(II) of unsupported RGO composites with different materials examined. B) Comparison of  $K_d$  values obtained for the adsorption of Hg(II) of supported RGO composite with RS, Ch, Ch@RS. C) Kinetics of Hg(II) adsorption by various adsorbents (temperature = 30 ± 2°C; pH = 7 ± 0.2, initial Hg(II) conc. = 1 mg/L). D) Performance comparison of RGO composites for removing Hg(II) from distilled water and real water (initial Hg(II) conc. = ~ 1 mg/L).

Figure 16. Pseudo-first-order kinetic plots with experimental data for adsorption of Hg(II) by GO, RGO and various RGO composites (E – experimental, P – predicted) A). unsupported and B) supported form. Table 1. Pseudo-first-order and pseudo-second-order rate parameters obtained for the adsorption of fluoride by various adsorbents.

Figure 17. Selectivity of adsorption of RGO-Ag for the indicated metal ions at three different initial concentrations (~ 1, 2 and 5 mg/L).

## DESCRIPTION WITH REFERENCE TO DRAWINGS AND TABULATED DATA

Figure 1 shows the UV/Vis spectral changes accompanied by the addition of different metal ions to RGO suspensions. All spectra were collected after 12 h of the addition of metal ion precursors. Figure 1 A show the spectral changes observed after the addition of  $\text{KMnO}_4$  to RGO solution. All the spectral features are marked in the figure. At lower concentrations, there is no peak corresponding to  $\text{KMnO}_4$  in the UV/Vis spectrum. The RGO peak at 270 nm as well as a broad peak characteristic of metal oxide, in this case  $\text{MnO}_2$ , can only be seen. A comparison of this peak with conventionally made  $\text{MnO}_2$  nanoparticles confirmed that the broad feature around 400 nm is indeed due to the formation of  $\text{MnO}_2$  nanoparticles. Literature too suggested that the spectral changes indicate the reduction of  $\text{KMnO}_4$  to colloidal  $\text{MnO}_2$  nanoparticles (Luo, Y., Preparation of  $\text{MnO}_2$  nanoparticles by directly mixing potassium permanganate and polyelectrolyte aqueous solutions. *Mater. Lett.* **2007**, 61, 1893). We can see that the  $\text{KMnO}_4$  feature at 565 nm begins to appear when the concentration of  $\text{KMnO}_4$  added reached 0.1 mM. It shows that at this concentration onwards, the reduction is incomplete. There was a blue shift for the graphenic peak at 270 as the concentration of  $\text{KMnO}_4$  added increased. This blue shift is an indication of the oxidation of RGO to GO (Sreeprasad, T. S., Samal, A. K., Pradeep, T., Tellurium nanowire-induced room temperature conversion of graphite oxide to leaf-like graphenic structures. *J. Phys. Chem C* **2009**, 113, 1727.). These results can be interpreted as the oxidation of graphene by  $\text{KMnO}_4$ , which makes GO and  $\text{MnO}_2$ . Figures 1 B-D show the UV/Vis spectral characteristics of the reduction of  $\text{Au}^{3+}$ ,  $\text{Ag}^+$  and  $\text{Pt}^{2+}$  by RGO. All the tested elements showed blue shift in the RGO

peak upon increasing the concentration of precursor ion added, pointing to oxidation of RGO.

Large area TEM images of the as-synthesized RGO (Figure 2) showed wrinkled sheets characteristics of graphenic structures (Gil, A. J., Adhikari, S., Scarpa, F., Bonet, J. The formation of wrinkles in single-layer graphene sheets under nanoindentation *J. Phys.: Condens. Matter.* **2010**, *22*, 145302.; Meyer, J. C., Geim, A. K., Katsnelson, M. I., Novoselov, K. S., Booth, T. J., Roth, S., The structure of suspended graphene sheets *Nature* **2007**, *446*, 60). The edges and wrinkles were measured to be around ~1-1.5 nm, close to a bilayer thickness (Gil, A. J., Adhikari, S., Scarpa, F., Bonet, J. The formation of wrinkles in single-layer graphene sheets under nanoindentation *J. Phys.: Condens. Matter.* **2010**, *22*, 145302.). After the formation of the composites also, structure of the RGO sheets remained the same (with wrinkles). We conclude that the composites are graphenic in nature with not more than two layers in thickness.

Figure 2C and 2D shows the TEM images taken from the RGO-MnO<sub>2</sub> sample. We can see large islands of MnO<sub>2</sub> nanoparticles on the RGO sheets and there are definite islands of nanoparticles of around 10 nm in size. Individual nanoparticles of smaller size regime (~5 nm) can also be seen. Inset of Figure 2D shows a lattice resolved image of the nanoparticle formed. The lattice was indexed to {100} and {110} planes of  $\delta$ -MnO<sub>2</sub> with a lattice spacing of 0.25 nm, and 0.14 nm, respectively (Feng, X. H., Zhai, L. M., Tan, W. F., Liu, F., He, J. Z., Adsorption and redox reactions of heavy metals on synthesized Mn oxide minerals. *Environ. Pollut.* **2007**, *147*, 366.). Figure 3 shows the TEM micrographs of RGO-Ag sample. Figure 3C shows a large area image and we can see that the particles are well separated, devoid of any aggregation. Particles are in the size range of 10-15 nm. Figure 3D shows a lattice resolved image of the nanoparticle. We can see that the formed nanoparticles are crystalline in nature. The {111} plane with a d-spacing of 0.235 nm characteristic of cubic Ag, is marked in the figure (Zhang, Y. X. L., S. H., DeAngelis, R. J., Lee, K. W., Reed, C. P., Nazareth, A., The process-controlled magnetic properties in nanostructured Fe/Ag composite films. *J. Appl. Phys.*

1991, 69, 5273). Typical of the nature of Ag nanoparticles, some polydispersity was seen at places.

Similarly, composites containing Au, Pt, and Pd were prepared and characterized using various microscopic techniques and is shown in Figures 4-6, respectively. At lower concentrations, the nanoparticles were monodispersed. But, as the concentration of the precursor increased, the size of the nanoparticle formed increased and the sample became progressively polydispersed. At higher concentrations, though the sample showed aggregation, a considerable amount of nanoparticles are observed (Figure 4-6). In the case of Pt and Pd composites, the aggregation was largely due to precursor acidity, which can be controlled, to some extent, by adjusting the precursor pH to near neutral. Although, all the tested metals showed an increase in particle size with the increase in precursor concentrations (Figure 4-6, Figure 7B<sub>1</sub>-B<sub>3</sub>), a different behavior was observed in the case of RGO-MnO<sub>2</sub> composite. Here, as the concentration of added KMnO<sub>4</sub> increased, the density of MnO<sub>2</sub> islands increased without much change in the particle size (Figures 7A<sub>1</sub>-A<sub>3</sub>).

Raman spectrum of the composite showed features of RGO as well as (Figure 8) MnO<sub>2</sub>. The presence of Mn-O vibration at 632 cm<sup>-1</sup> confirmed the presence of MnO<sub>2</sub> in the composite and based on previous reports, the phase present may be  $\delta$ -MnO<sub>2</sub> (Liang, S., Teng, F., Bulgan, G., Zong, R., Zhu, Y., Effect of Phase Structure of MnO<sub>2</sub> Nanorod Catalyst on the Activity for CO Oxidation. *Format. J. Phys. Chem. C* **2008**, 112, 5307.; Buciuman, F. P., F., Craciun, R., Zahn, D. R. T., Vibrational spectroscopy of bulk and supported manganese oxides. *Phys. Chem. Chem. Phys.* **1999**, 1, 185.). Raman features of  $\delta$ -MnO<sub>2</sub> are comparatively weaker (Liang, S., Teng, F., Bulgan, G., Zong, R., Zhu, Y., Effect of phase structure of MnO<sub>2</sub> nanorod catalyst on the activity for CO oxidation. *J. Phys. Chem. C* **2008**, 112, 5307.) and the amount of MnO<sub>2</sub> presents in the composite being minimal; all the vibrations were not seen.

Figure 9 shows the expanded view of the Raman spectra obtained from the composite, in the region of D- and G-band of graphene, having different metal content. In a typical



synthesis, GO showed D-band at  $1345\text{ cm}^{-1}$  and G-band at  $1598\text{ cm}^{-1}$ . After the reduction to RGO, the D-band remained the same but G-band shifted to lower frequency region and was observed at  $1580\text{ cm}^{-1}$ . Both these positions are marked by vertical lines in the spectra. The Raman spectra of the composites showed interesting observations. From the spectra we can see that the D-band remained the same irrespective of the increase in  $\text{KMnO}_4$  concentration (Figure 9A). But the G-band underwent some changes. As the concentration of  $\text{KMnO}_4$  increased, the G-band shifted to higher frequency region with respect to RGO. As the concentration reached  $0.1\text{ mM}$ , the G-band position was more or less similar to that of GO implying the oxidation of graphene to GO by  $\text{KMnO}_4$ . This implies a redox-like reaction between RGO and  $\text{KMnO}_4$  which results in the oxidation of RGO to GO and the reduction of  $\text{KMnO}_4$  to  $\text{MnO}_2$  nanoparticles. As the concentration of  $\text{KMnO}_4$  increases, it uses up more RGO and gets converted to  $\text{MnO}_2$ . As a result, more and more RGO get oxidized and it is shown in the Raman spectrum by the blue-shift in the G-band with respect to RGO (Sreeprasad, T. S., Samal, A. K., Pradeep, T., Tellurium nanowire-induced room temperature conversion of graphite oxide to leaf-like graphenic structures. *J. Phys. Chem. C* **2009**, *113*, 1727.). In the case of silver composite (Figure 9B) also similar change was observed. But in here, the extent of oxidation was lesser for the same concentration of metal content, compared to  $\text{KMnO}_4$ . This is understandable, since the reduction of Ag (+1) to Ag (0) requires only lesser number of electrons compared to the reduction of Mn (+7) to Mn (+4). So the corresponding oxidation happening to RGO will also be lesser.

Figure 10 shows the XPS spectra of samples containing different loadings of Mn. Upon increasing the precursor,  $\text{KMnO}_4$  concentration, the feature of Mn in the spectra became more prominent, implying the reduction of  $\text{KMnO}_4$  (Figure 10  $\text{C}_1$  to  $\text{C}_3$ ). In all the samples, Mn  $2p_{3/2}$  peak was centered around  $641.8\text{ eV}$  while the Mn  $2p_{1/2}$  peak was around  $653.5\text{ eV}$ . There was no feature observed around  $647\text{ eV}$  corresponding to the Mn  $2p_{3/2}$  signal of  $\text{KMnO}_4$  confirming the complete reduction of  $\text{KMnO}_4$  to  $\text{MnO}_2$  nanoarticles. The  $\Delta J$  of  $11.6\text{ eV}$  again confirmed that the formed species is  $\text{MnO}_2$ . The corresponding oxidation was seen in carbon  $1s$  and oxygen regions. In the first sample,

the carbon spectrum was having only very less extent of oxidation (Figure 10A<sub>1</sub>). But, as the concentration of KMnO<sub>4</sub> added increased, the signatures of oxidation in carbon also increased. All oxygenated features increased in intensity as the concentration of KMnO<sub>4</sub> added into RGO increased. Similar trend was observed in the O 1s spectra as well. Upon deconvolution, each sample showed three components. First component centered around 530 eV. Metal oxides are known to show the O 1s feature around 530 eV (Yujie, X., Yi, X., Zhengquan, L., Changzheng, W., Growth of well-aligned  $\delta$ -mno<sub>2</sub> monocrystalline nanowires through a coordination-polymer-precursor route. *Chem. Eur. J* **2003**, *9*, 1645.). In all the samples analyzed, one component was always resolved around 530 eV confirming the presence of MnO<sub>2</sub> nanoparticle in the sample. Oxygen in carbonyl (C=O) and carboxylate functionalities (O=C–OH) in GO is also known to give features around 530 eV (Yang, Y.; Wang, J.; Zhang, J.; Liu, J.; Yang, X.; Zhao, H. Exfoliated graphite oxide decorated by PDMAEMA chains and polymer particles. *Langmuir* **2009**, *25*, 11808.; Cecilia, M.; Goki, E.; Stefano, A.; Steve, M.; Mkhoyan, K. A.; Ozgur, C.; Daniel, M.; Gaetano, G.; Eric, G.; Manish, C. Evolution of electrical, chemical, and structural properties of transparent and conducting chemically derived graphene thin films. *Adv. Funct. Mater.* **2009**, *19*, 2577.; Yang, D., Velamakanni, A., Bozoklu, G., Park, S., Stoller, M., Piner, R. D., Stankovich, S., Jung, I., Field, D. A., Ventrice Jr, C. A., Ruoff, R. S., Chemical analysis of graphene oxide films after heat and chemical treatments by X-ray photoelectron and Micro-Raman spectroscopy. *Carbon* **2009**, *47*, 145.). The second component centered around 532 eV is reported to be due to the hydroxyl oxygen (C–OH) in graphene (Cecilia, M., Goki, E., Stefano, A., Steve, M., Mkhoyan, K. A., Ozgur, C., Daniel, M., Gaetano, G., Eric, G., Manish, C., Evolution of electrical, chemical, and structural properties of transparent and conducting chemically derived graphene thin Films. *Adv. Funct. Mater.* **2009**, *19*, 2577.; Yang, D., Velamakanni, A., Bozoklu, G., Park, S., Stoller, M., Piner, R. D., Stankovich, S., Jung, I., Field, D. A., Ventrice Jr, C. A., Ruoff, R. S. Chemical analysis of graphene oxide films after heat and chemical treatments by X-ray photoelectron and Micro-Raman spectroscopy. *Carbon* **2009**, *47*, 14.). The third component around 533 eV may be due to adsorbed water or due to C–O (Cecilia, M., Goki, E., Stefano, A., Steve, M., Mkhoyan, K. A., Ozgur, C., Daniel, M., Gaetano, G., Eric, G., Manish, C. Evolution of electrical,

chemical, and structural properties of transparent and conducting chemically derived graphene Thin Films. *Adv. Funct. Mater.* **2009**, *19*, 2577.; Yang, D., Velamakanni, A., Bozoklu, G., Park, S., Stoller, M., Piner, R. D., Stankovich, S., Jung, I., Field, D. A., Ventrice Jr, C. A., Ruoff, R. S., Chemical analysis of graphene oxide films after heat and chemical treatments by X-ray photoelectron and Micro-Raman spectroscopy. *Carbon* **2009**, *47*, 145.). Based on these observations, we can propose a redox-like reaction in which the RGO is getting oxidized and  $\text{KMnO}_4$  is getting reduced to  $\text{MnO}_2$  nanoparticles. The RGO-Ag composite was also analyzed by XPS (Figure 11). This also showed that as the concentration of  $\text{AgNO}_3$  increased, the oxidation of carbon got increased. But, similar to the observation in Raman, the extent of oxidation was much lesser compared to the  $\text{MnO}_2$  composite, supporting our proposition. The metal composites were analyzed by EDX also. All the EDX spectra showed metal content and the corresponding imaging showed distribution of particles on the RGO sheets which had a one to one correspondence with the corresponding TEM images.

In order to employ any nanomaterials in the field for water purification, the materials have to be supported on suitable substrates. Here, RGO nanocomposites were supported on RS using chitosan as the binder. Figure 12A shows the SEM images of Ch-RGO-Ag@RS. The particles are micrometers in size and can settle easily by sedimentation. Inset photograph shows the SEM image of virgin RS. Figure 12B shows the SEM image of Ch-RGO- $\text{MnO}_2$ @RS. EDAX analysis revealed the presence of Ag and  $\text{MnO}_2$  on the surface of RS (Figures 13 and 14). The presence of chitosan was confirmed by the nitrogen signal in both composites. The supported composites were also characterized by Raman spectroscopy (Figure 12C). All the composite showed a fluorescence background. This may be attributed to the presence of chitosan. The presence of Si-O bending ( $440\text{ cm}^{-1}$ ) (Hemley, R. J., Mao, H. K., Bell, P. M., Mysen, B. O., Raman spectroscopy of  $\text{SiO}_2$  glass at high pressure *Phys. Rev. Lett.* 1986, *57*, 747). In all the above composites confirmed the presence of  $\text{SiO}_2$ . The clear features of RGO (broad D and G band) were evident in both Ch-RGO- $\text{MnO}_2$ @RS and Ch-RGO-Ag@RS, indicating that RGO is effectively immobilized on RS surface. Characteristic Mn-O ( $630\text{ cm}^{-1}$ ) (Liang, S., Teng, F., Bulgan, G., Zong, R., Zhu, Y., Effect of phase structure of

MnO<sub>2</sub> nanorod catalyst on the activity for CO oxidation. *J. Phys. Chem. C* **2008**, 112, 5307.). vibration in Ch-RGO-MnO<sub>2</sub>@RS confirms the presence of MnO<sub>2</sub> nanoparticles in the composite. Photograph in Figure 12D shows clear change in color after the incorporation of composites. The color of RS changed from pale yellow to brown upon coating of RGO composites.

### **Environmental remediation application of RGO composites**

Here, RGO, and its composites were tested for Hg(II) uptake. A few other adsorbents were also compared. Distribution coefficient,  $K_d$  is an important parameter to compare the affinity of a pollutant to an adsorbent. It is possible to compare the effectiveness of the adsorbent by comparing the magnitude of the  $K_d$  value. Higher the  $K_d$  value, the more effective the adsorbent material is. In general, the  $K_d$  values of  $\geq 1$  L/g are considered good, and those above 10 L/g are outstanding. (Yantasee, W., Warner, C. L., Sangvanich, T., Addleman, R. S., Carter, T. G., Wiacek, R. J., Fryxell, G. E., Timchalk, C., Warner, M. G., Removal of heavy metals from aqueous systems with thiol functionalized superparamagnetic nanoparticles. *Environ. Sci. Technol.* **2007**, 41, 5114.; Fryxell, G. E., Lin, Y., Fiskum, S., Birnbaum, J. C., Wu, H., Kemner, K., Kelly, S., Actinide sequestration using self-assembled monolayers on mesoporous supports. *Environ. Sci. Technol.* **2005**, 39, 1324.). The  $K_d$  values calculated at equilibrium clearly indicate that RGO-MnO<sub>2</sub> and RGO-Ag, both supported and unsupported forms, are excellent candidates for Hg(II) removal (Figure 15A and B). The RGO composites outperformed all other materials studied. The importance of RGO as a substrate is also well demonstrated.  $K_d$  values showed that the nanoparticles in supported state in graphene composites are 10 times better candidates. On close comparison of  $K_d$  value (without considering the weight of sand), we see that RGO-composites in the supported form are superior (4-5 times increase in  $K_d$  values) in removing Hg(II) compared to unsupported RGO-composites. This enhancement in affinity could be due to the synergetic effect arisen from the combination of materials.

Kinetic study was performed to understand the time dependant removal of Hg(II) by few selected adsorbents including GO, RGO, RGO-MnO<sub>2</sub>, RGO-Ag, Ch-RGO-MnO<sub>2</sub>@RS, and Ch-RGO-Ag@RS. Figure 15C shows that all the tested materials are capable of adsorbing Hg(II) from water. Pristine RGO and GO showed similar kinetics of removal and did not show any significant variation in equilibrium uptake capacity. Compared to the parent material, RGO-composites showed higher removal kinetics and the system could remove Hg(II) completely from the aqueous medium. The RGO-composites supported on RS also showed higher uptake rate and it is superior to all other adsorbent materials tested.

To quantify the uptake rate, which is important in engineering design, the experimental kinetic data were analyzed with commonly used reaction kinetic models such as Lagergren pseudo-first-order (Lagrange, S. Zur theorie der sogenannten adsorption gelöster stoffe *K Sven.Vetenskapsakad.* **1898**, 24, 1).and Ho's pseudo-second-order (Ho, Y. S.; McKay, G. The kinetics of sorption of divalent metal ions onto sphagnum moss peat reaction rate models. *Water Res.* **2000**, 34, 735.). Mathematical representations of these models are given below.

Pseudo-first-order equation: 
$$q_t = q_e (1 - e^{-k_1 t}) \quad (1)$$

Pseudo- second-order equation: 
$$q_t = \frac{q_e^2 k_2 t}{1 + q_e k_2 t} \quad (2)$$

Where  $q_e$  and  $q_t$  are the adsorption capacity at equilibrium and at time  $t$ , respectively (mg/g).  $k_1$  is the rate constant of pseudo-first-order adsorption (1/min) and  $k_2$  is the rate constant of pseudo-second-order adsorption (g/mg min).

A non-linear approach was used to find the best-fitting model and kinetic parameters. The model predicted kinetic parameters and their associated error measurements show that pseudo-first-order equation is more appropriate in predicting the experimental data (Figure 16). The pseudo-first order model predicted plots with experimental data are given in Figure 16A and B.



In order to evaluate the Hg(II) removal capability of the RGO-composites, both supported and unsupported in real water, a groundwater spiked with ~1 mg/L of Hg(II) was prepared and tested for uptake. Control experiments were also conducted with ~1 mg/L Hg(II) spiked distilled water. The results obtained from these experiments are shown in Figure 15. The data clearly established that complete (below detectable limit) removal of Hg(II) happened in both the systems. The co-ions present in the real sample did not affect the removal, indicating that such a system can be employed for the applications of real water. However, more investigations are needed to establish the extent of Hg(II) removal under various conditions.

For checking the selectivity of the RGO-composites for Hg(II), batch adsorption experiments were conducted in distilled water by spiking a mixture of metal ions, including Hg(II), Ni(II), Cu(II) and Cd(II). Three sets of studies were conducted and each set of experiment was performed by using a mixture of aqueous solution of ~ 1 mg/L, 2 mg/L and 5 mg/L each four metal ions mentioned above. The selectivity data obtained for the RGO-Ag system is depicted in Figure 17. The results reveal that RGO-Ag system is highly selective for the Hg(II) and the selectivity varied as per the order; Hg(II)<Cu(II)<Ni(II)<Cd(II). However, Hg(II) removal by RGO-MnO<sub>2</sub> system is significantly affected by the presence of other metal ions. The difference in selectivity pattern observed in the case of two composites may be due to difference in chemical selectivity of the metal/metal oxide used in the composites towards the target contaminants. MnO<sub>2</sub> is known to remove a wide range of cations and the main adsorption mechanism responsible for the removal is electrostatic interaction between the adsorbate and the adsorbent. Hence, a reduction in uptake of target contaminant (Hg(II)) is expected in presence of other cations (Lisha, K. P., Maliyekkal, S. M., Pradeep, T., Manganese dioxide nanowhiskers: A potential adsorbent for the removal of Hg(II) from water. *Chem. Engg. J.* **2010**, *160*, 432.). The selectivity of RGO-Ag system for Hg(II) may be due to the higher affinity of Ag towards Hg(II) (Bootharaju, M. S., Pradeep, T., Uptake of toxic metal ions from water by naked and monolayer protected silver nanoparticles: An X-ray photoelectron spectroscopic investigation *J. Phys. Chem. C* **2010**, *114*, 8328).

In summary, utilizing the reducing capacity of RGO, different metal/metal oxide composites were prepared. Based on different spectroscopic and microscopic evidences, the formation was established to be due a redox-like reaction between RGO and the metal precursor. The oxidation of RGO mainly results in GO and metal precursors are getting reduced into the corresponding nanoparticles which are attached onto the RGO sheets, as evident from TEM and SEM. Heavy metal scavenging capacity of the as prepared materials were demonstrated taking Hg(II) as the model pollutant. Considering the practical difficulty in applying nanomaterial for water purification, attempts were also made to immobilize the RGO composites on a cheap support like RS and the supported material was tested for Hg(II) uptake. The composite materials were found to be excellent candidates for Hg(II) removal from water.

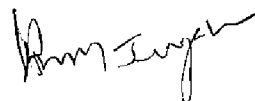
**We Claim:**

1. A method of preparing reduced graphene oxide (RGO)-metal/metal oxide nanocomposites in water using the inherent reducing ability of RGO and without any external reducing aid(s), at room temperature, with metal or metal oxide particles size below 100 nm, wherein
  - (a) the metal precursor includes but not limited to silver nitrate, chloroauric acid, potassium permanganate,  $\text{PdCl}_2$ ,  $\text{H}_2\text{PtCl}_6$ ,  $\text{CrO}_3$ , aquapentamine Co(III) chloride or a combination thereof.
  - (b) the RGO is prepared through chemical, physical or hydrothermal process.
  - (c) the metal reduction and subsequent formation of metal or metal oxide nanoparticles is carried out in-situ by RGO.
  - (d) the reduction of metal precursor by RGO is carried out at temperature  $<40^\circ\text{C}$ .
2. A method as claimed in claim 1, wherein the nanocomposite is prepared by the simultaneous reduction of metal/metal oxide precursor and graphene oxide.
3. A method as claimed in claim 1, wherein the nanocomposite is prepared by mixing the pre-formed metal/metal oxide nanoparticles and RGO at room temperature ( $<40^\circ\text{C}$ ).
4. A method as claimed in claim 1, wherein the size of the metal or metal oxide particles in the composites can be tuned by adjusting the precursor concentration.
5. An adsorbent composition having RGO-metal/metal oxide nanocomposites as claimed in claim 1, wherein the adsorbent composition is used for the removal of heavy metals from water including but not limited to Cu(II), Ni(II), Cd(II) and Hg(II).
6. A method as claimed in claim 1, wherein the metal precursor is selected from a group comprising of compounds including but not limited to, gold, silver, platinum, palladium, cobalt, manganese, iron, titanium, zirconium, lanthanum, cerium, or a combination thereof.
7. A method as claimed in claim 1, wherein the counter ions in the metal precursors include but not limited to chloride, nitrate, acetate, sulfate, bicarbonate or combination thereof.
8. A method as claimed in claim 1, wherein the graphene is used in the solid form or in the dispersed form or supported form prepared through physical, chemical, photochemical or hydrothermal process.
9. A method as claimed in claim 1, wherein the nanocomposite comprises at least one of RGO-Ag, RGO-Au, RGO-Pt, RGO-Pd, RGO-Fe, RGO-Rh, RGO-MnO<sub>x</sub>, RGO-CoO, RGO-TeO<sub>2</sub>, RGO-Ce<sub>2</sub>O<sub>3</sub>, RGO-Cr<sub>2</sub>O<sub>3</sub>.

10. A method as claimed in claim 1, wherein the nanocomposite is supported on a substrate comprising at least one of activated alumina, activated carbon, cellulose fibers, coconut fibers, clay.
11. A method as claimed in claim 1, wherein the nanocomposite is supported on a substrate by using at least one of chitosan, polyaniline, polyvinyl alcohol, and polyvinylpyrrolidone(PVP).
12. An adsorbent composition as claimed in claim 5, wherein the adsorbent is used as a filter in a filtering device in a variety of formats including but not limited to candle, molded porous block, filter bed, column, packets and bags.
13. An adsorbent composition as claimed in claim 5, wherein the adsorbent is used as a water treatment medium for water sources including but not limited to ground water sources, industrial sources and municipal sources.
14. An adsorbent composition as claimed in claim 5, wherein the adsorbent reduces heavy metals from media other than water.

Dated at Chennai this March 31, 2017

Signature:



D. Moses Jeyakaran  
Advocate & Patent Agent  
IN/PA — 369

## REDUCED GRAPHENE OXIDE-BASED-COMPOSITES FOR THE PURIFICATION OF WATER

### ABSTRACT

This invention describes a versatile, in-situ soft chemical synthetic route for the preparation of various graphene-metal and metal oxide composites. We suggest the use of such composites for water purification, one of the oldest and most commonly used applications of carbon materials, especially of relevance to poor countries. The inherent reduction ability of reduced graphene oxide (RGO) has been utilized to produce the composite structure from the respective precursor ions. The composites are found to be about one order of magnitude better compared to parent RGO and graphite oxide (GO) for this application. To make the composites adaptable for the application like water purification, they were immobilized on river sand (RS) using an environment friendly material, chitosan as the binder. The supported composites showed good stability and enhanced uptake capacity compared to unsupported composites, suggesting their utility in the field. The in-situ reduction strategy, without the aid of any external reducing agents seems to be convenient, cheap and eco-friendly and opens up several application possibilities in diverse fields of environmental relevance.



3 SEP 2010

ORIGINAL

2563 ICHE/ 2010

Name of the applicant:

Indian Institute of Technology Madras.

App. No.

No. of sheets: 44

Sheet No. 28

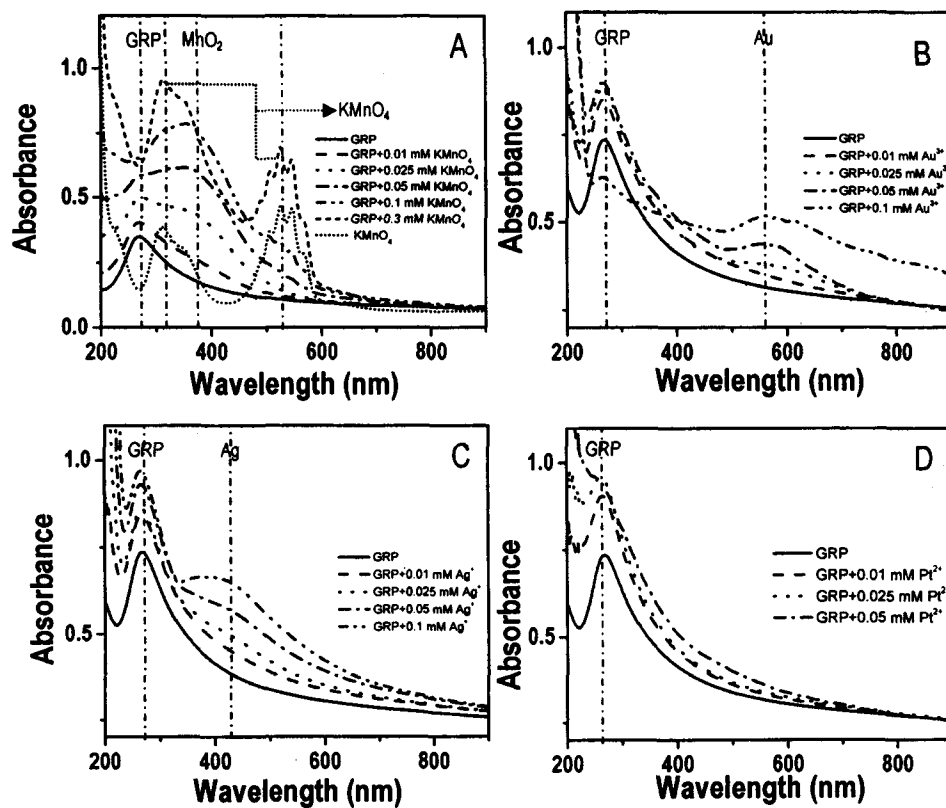


Figure 1.

Signature of the applicant:

Name of the applicant:

Indian Institute of Technology Madras.

App. No.

No. of sheets: 44

Sheet No. 29

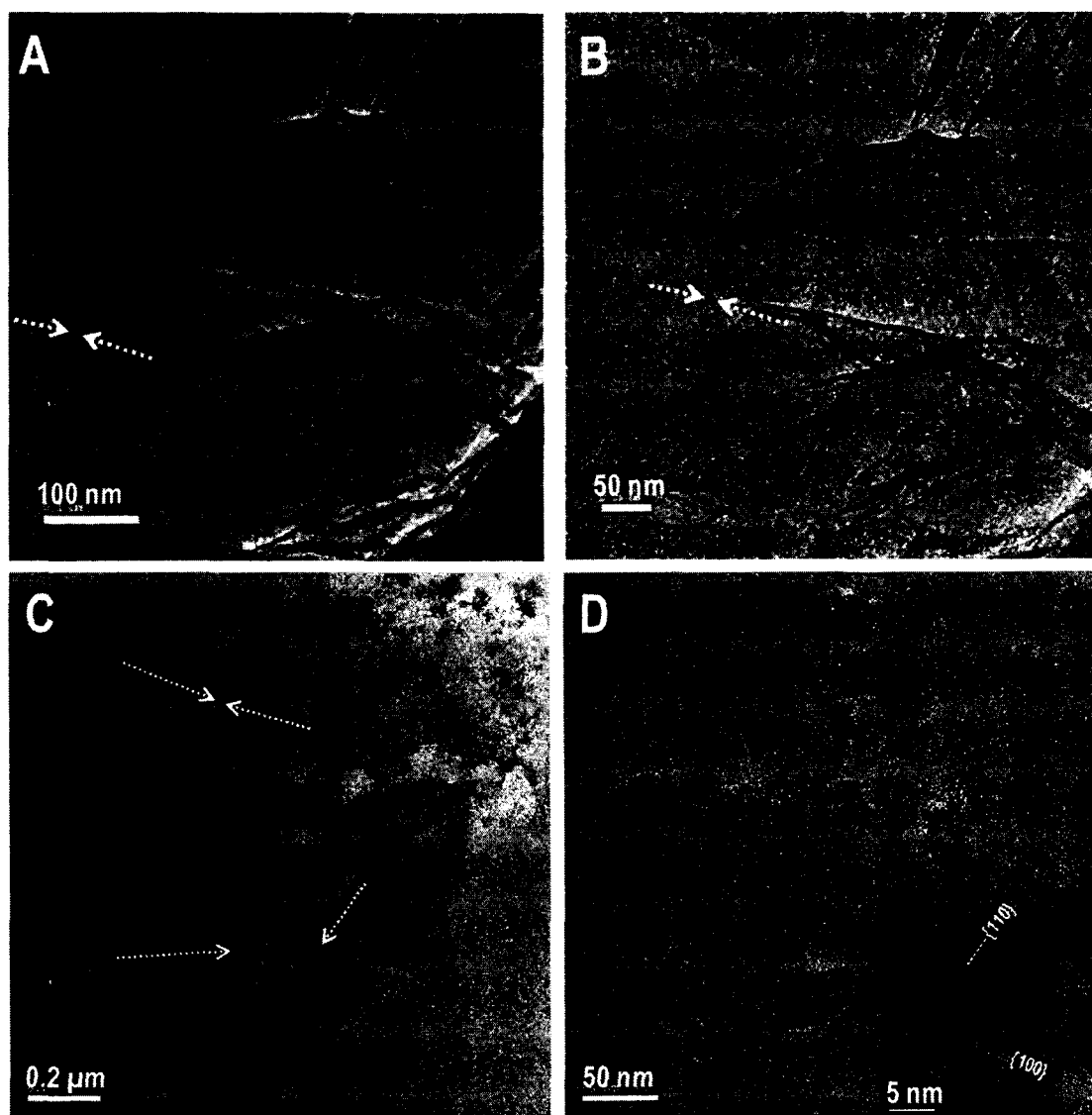


Figure 2

Signature of the applicant:

Name of the applicant:

No. of sheets: 44

Indian Institute of Technology Madras.

Sheet No. 30

App. No.

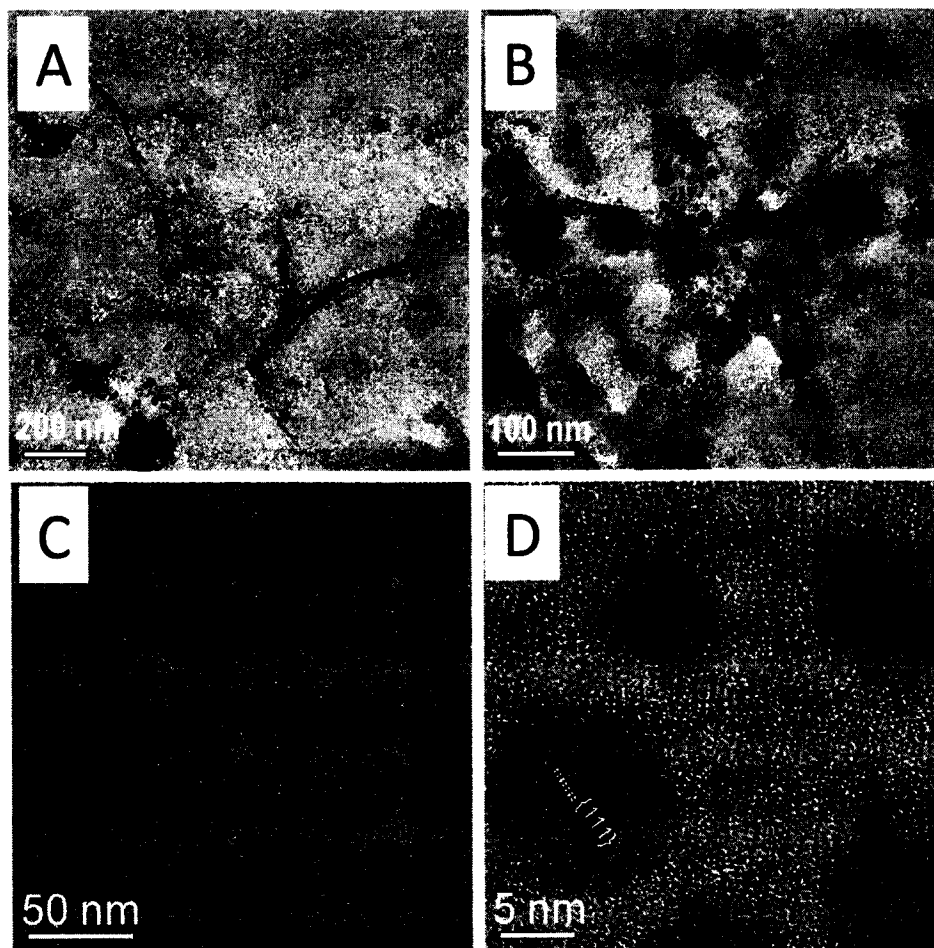


Figure 3.

  
Signature of the applicant:

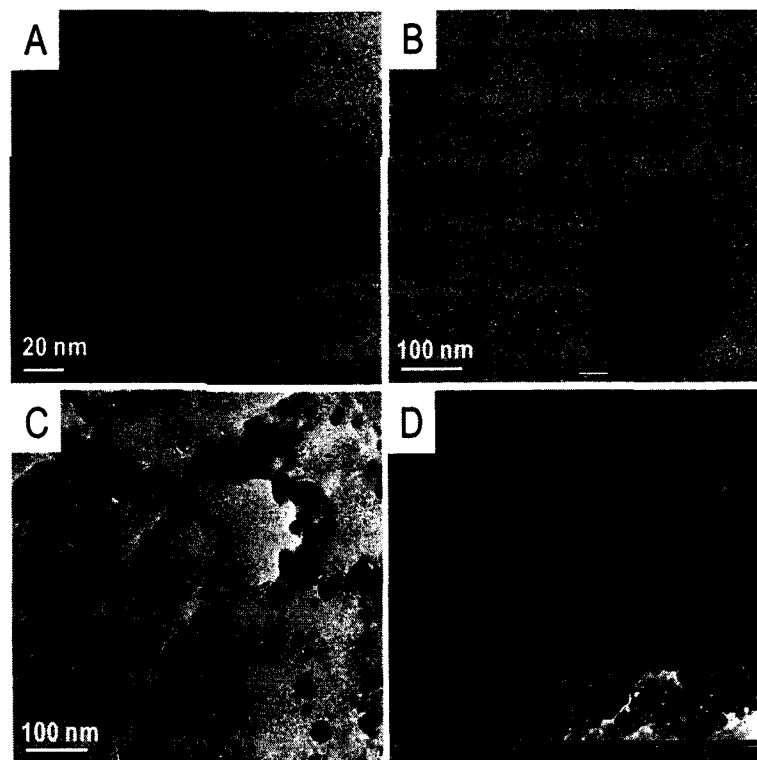
Name of the applicant:

No. of sheets: 44

Indian Institute of Technology Madras.

Sheet No. 31

App. No.



Figures 4

Signature of the applicant:

Name of the applicant:

No. of sheets: 44

Indian Institute of Technology Madras.

Sheet No. 32

App. No.

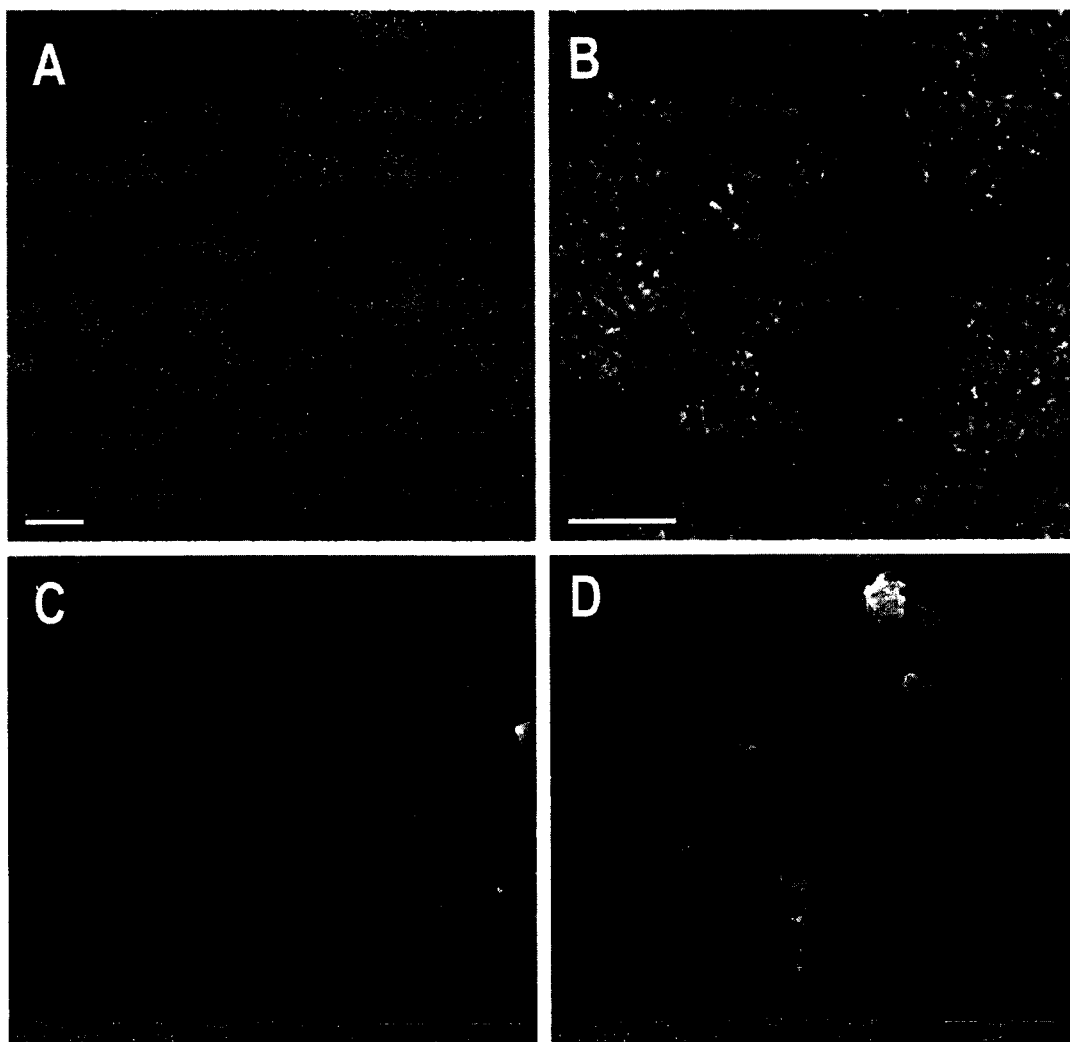


Figure 5

Signature of the applicant:

Name of the applicant:

No. of sheets: 44

Indian Institute of Technology Madras.

Sheet No.33

App. No.

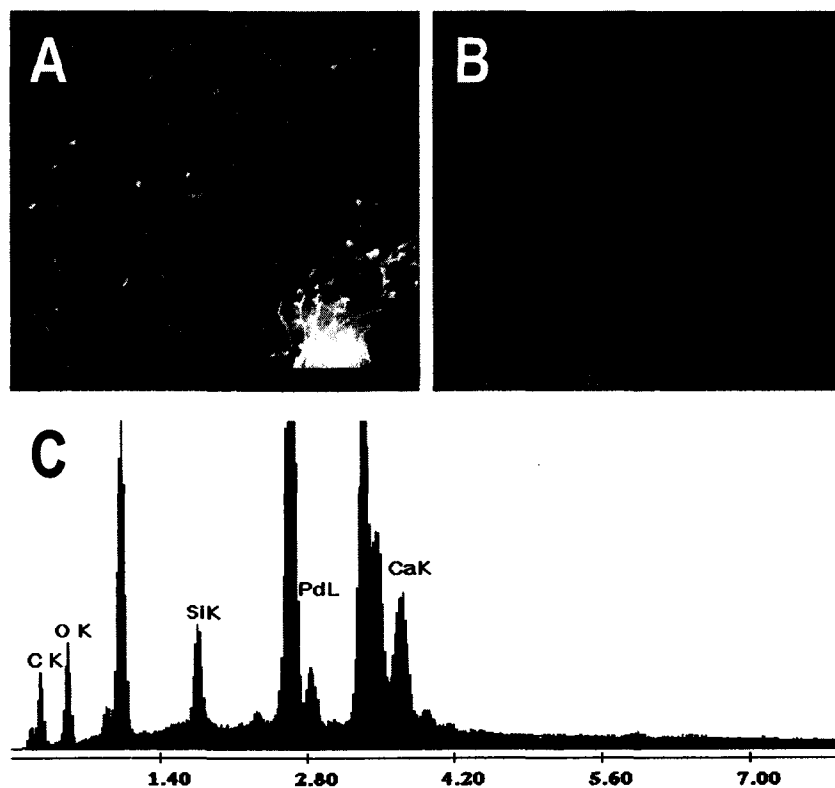


Figure 6

Signature of the applicant:

Name of the applicant:

No. of sheets: 44

Indian Institute of Technology Madras.

Sheet No. 34

App. No.

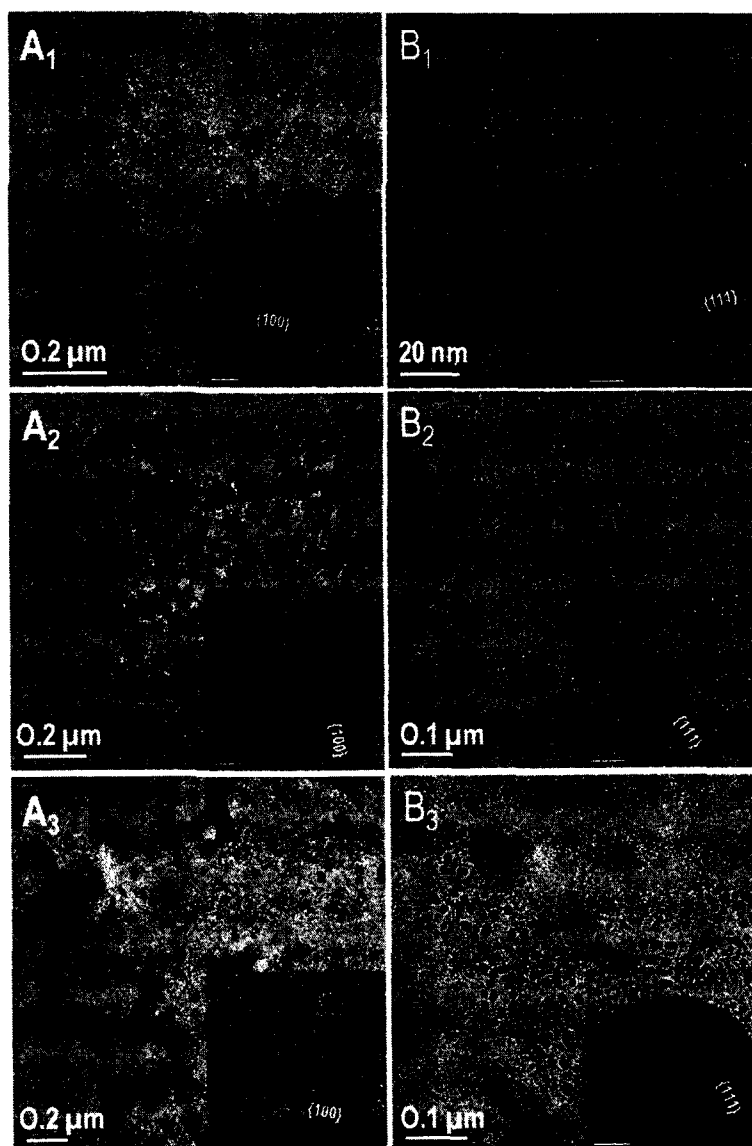


Figure 7

Signature of the applicant:

Name of the applicant:

No. of sheets: 44

Indian Institute of Technology Madras.

Sheet No. 35

App. No.

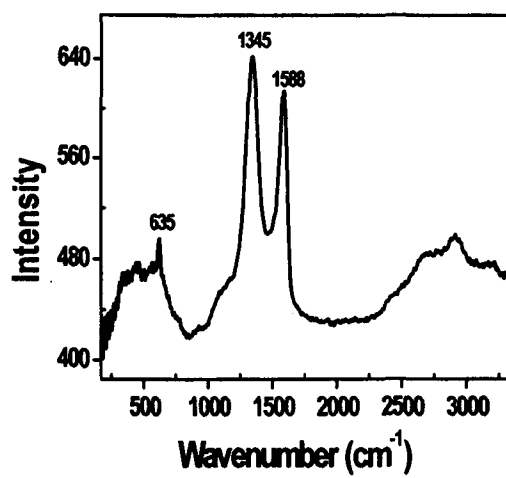


Figure 8

Signature of the applicant:



Name of the applicant:

No. of sheets: 44

Indian Institute of Technology Madras.

Sheet No. 36

App. No.

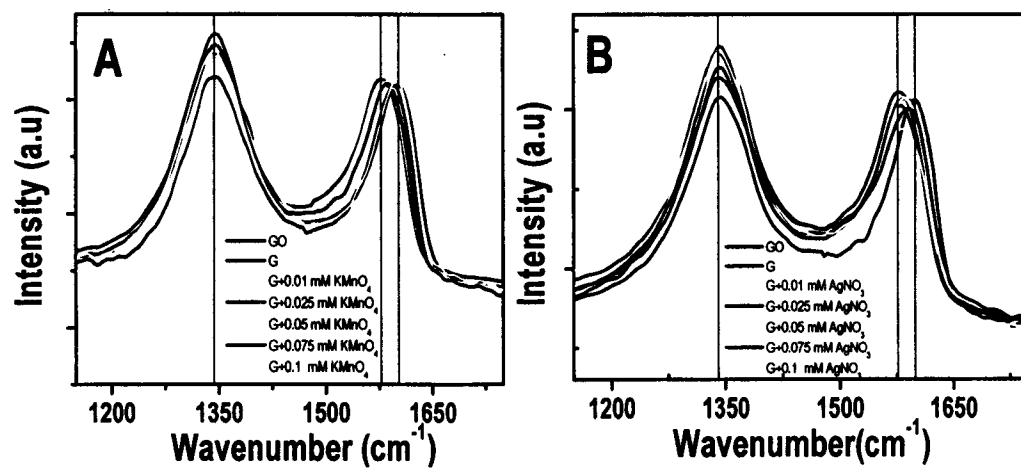


Figure 9.

Signature of the applicant:

Name of the applicant:

No. of sheets: 44

Indian Institute of Technology Madras.

Sheet No. 37

App. No.

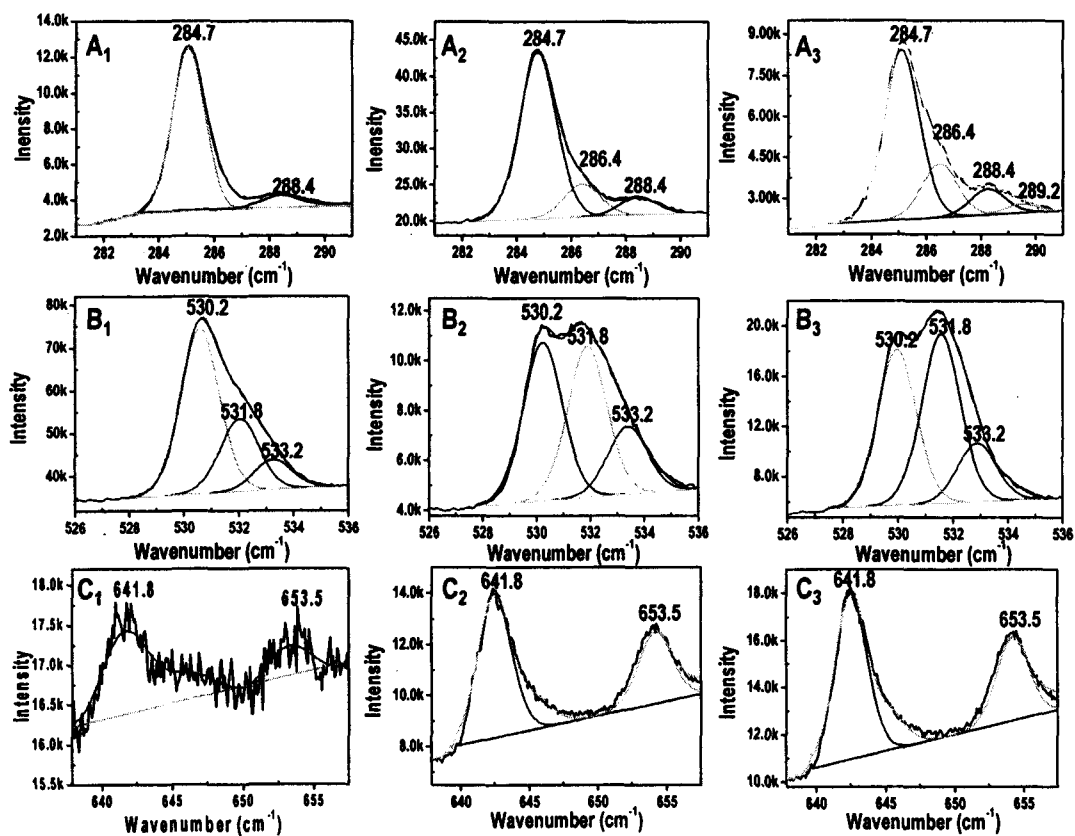


Figure 10

Signature of the applicant:

Name of the applicant:

No. of sheets: 44

Indian Institute of Technology Madras.

Sheet No. 38

App. No.

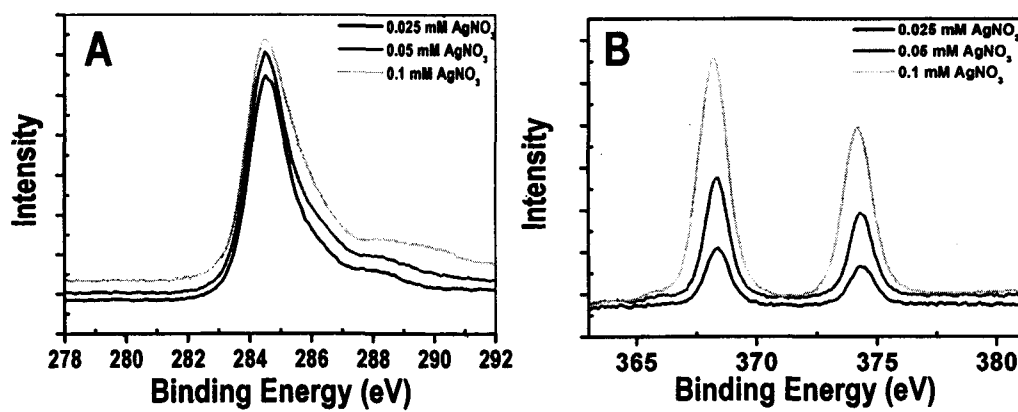


Figure 11

Signature of the applicant:

Name of the applicant:

No. of sheets: 44

Indian Institute of Technology Madras.

Sheet No. 39

App. No.

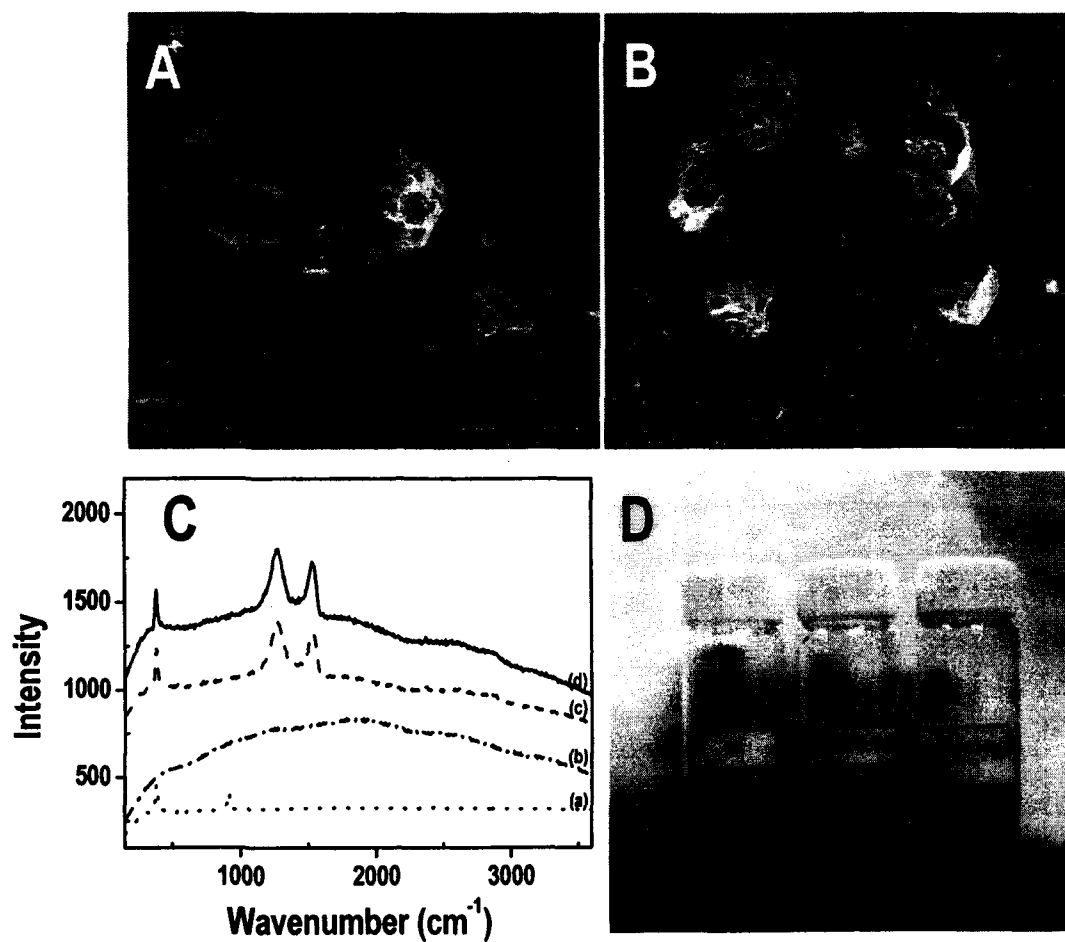


Figure 12.

Signature of the applicant:

Name of the applicant:

No. of sheets: 44

Indian Institute of Technology Madras.

Sheet No. 40

App. No.

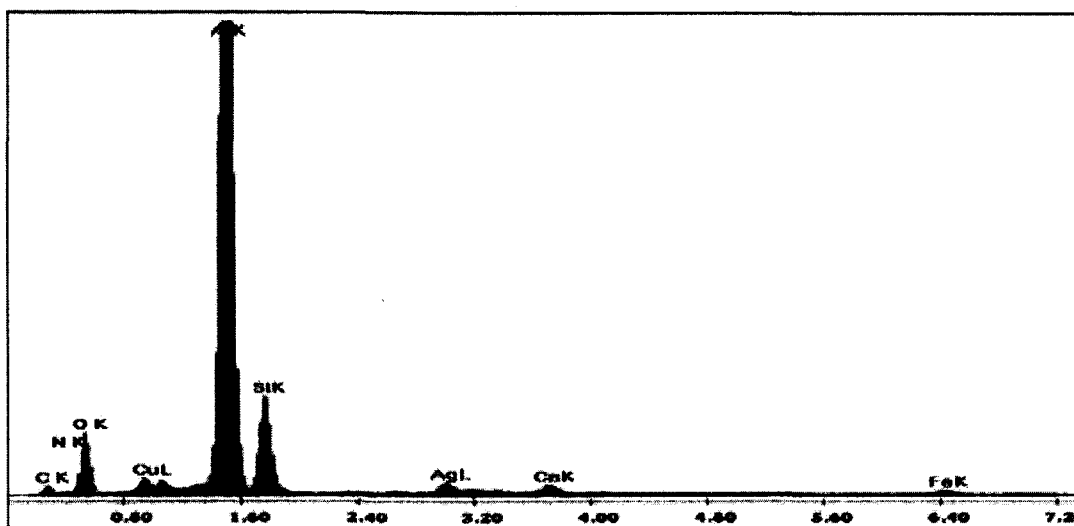
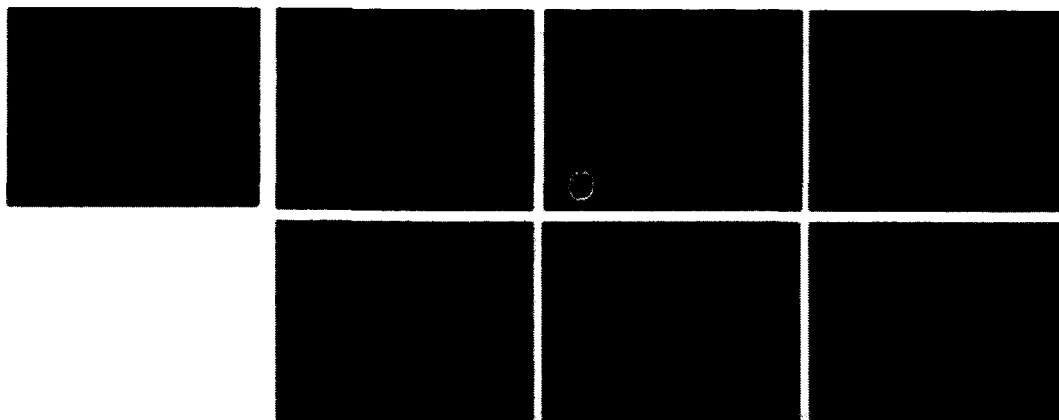


Figure 13

  
Signature of the applicant:

Name of the applicant:

No. of sheets: 44

Indian Institute of Technology Madras.

Sheet No. 41

App. No.

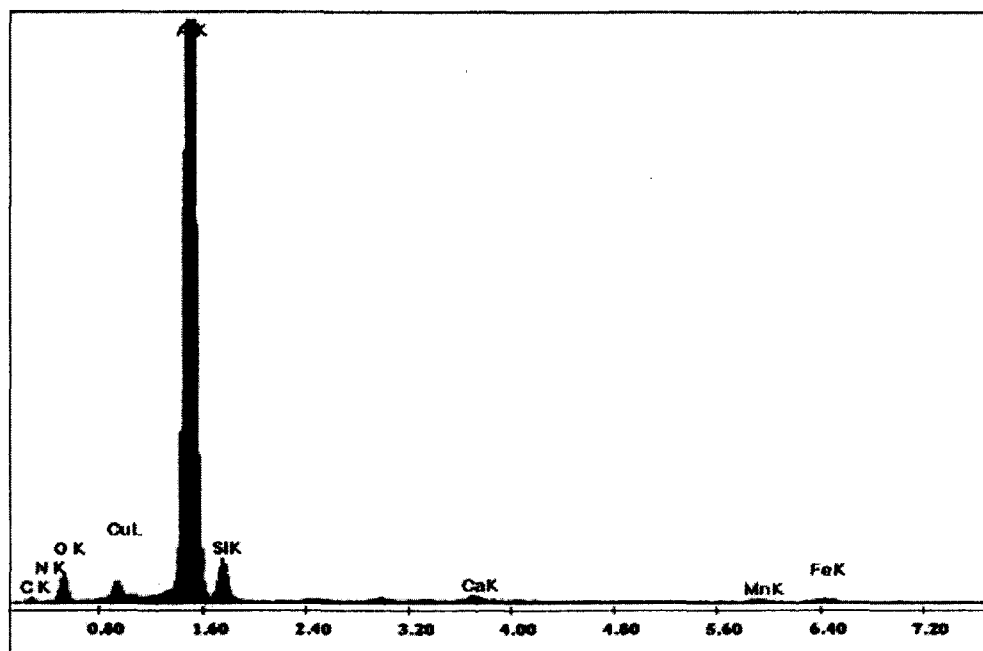
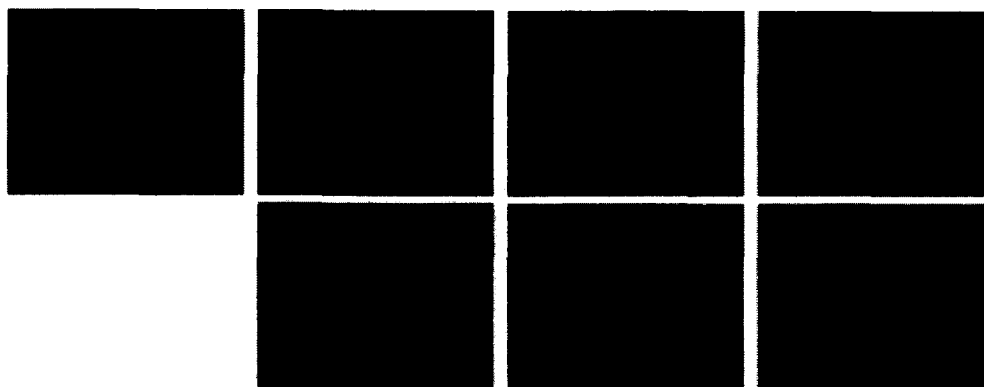



Figure 14

  
Signature of the applicant:

Name of the applicant:

No. of sheets: 44

Indian Institute of Technology Madras.

Sheet No. 42

App. No.

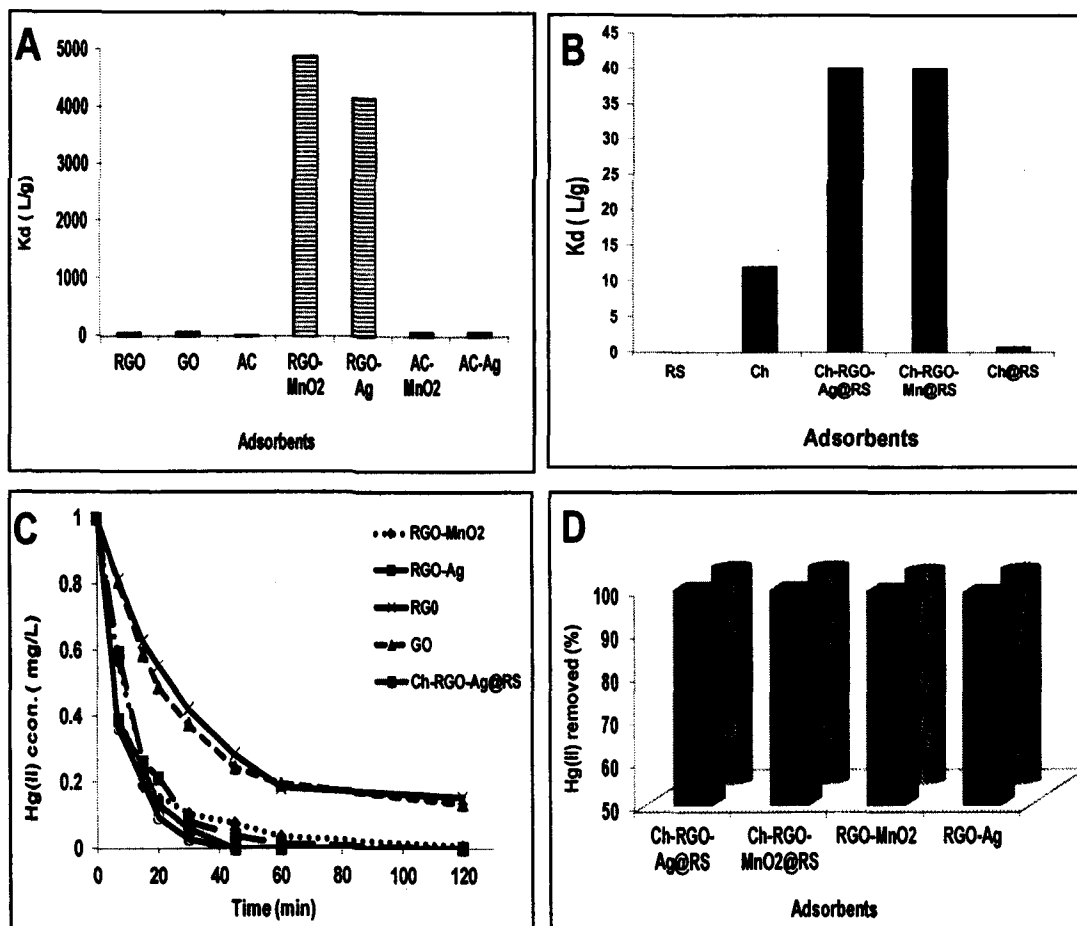


Figure 15.

Signature of the applicant:

Name of the applicant:

No. of sheets: 44

Indian Institute of Technology Madras.

Sheet No. 43

App. No.

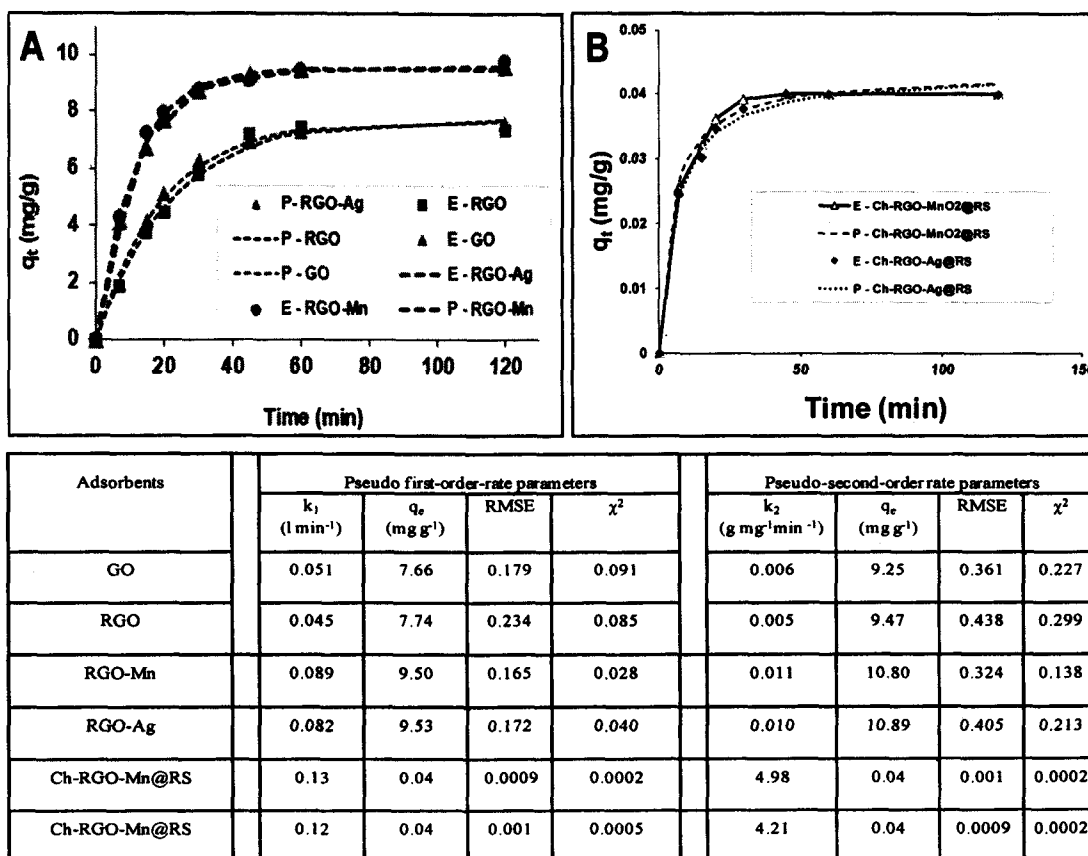


Figure 16.

Signature of the applicant:



Name of the applicant:

No. of sheets: 44

Indian Institute of Technology Madras.

Sheet No. 44

App. No.

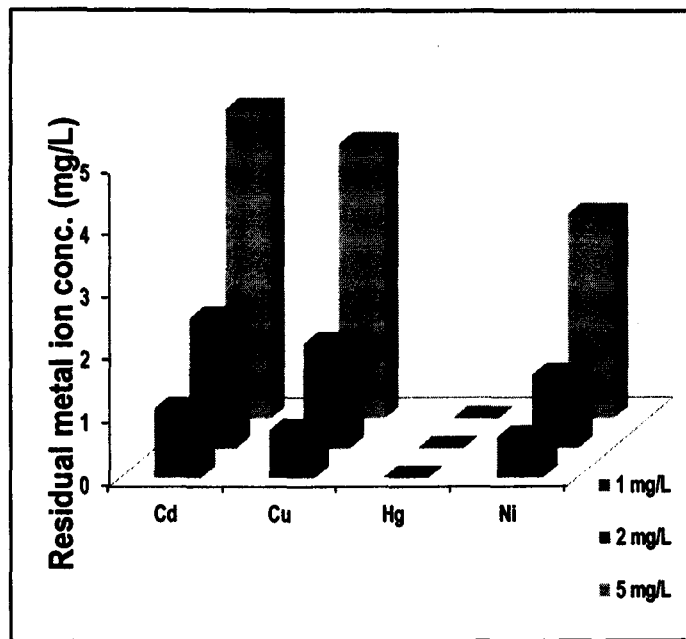


Figure 17

Signature of the applicant: